Real-Time Particle Tracking using a Formation of UAVs ⋆

Espen Oland Raymond Kristiansen

Narvik University College, Department of Technology, 8505 Narvik, Norway (e-mail: {eol},{rayk}@hin.no).

Abstract: In this paper the problem of real-time particle tracking is studied. Using sensor measurements, a formation of UAVs autonomously find the closest point with high particle density where they enter a holding pattern. After converging to the holding pattern, one UAV will remain, while the rest will go looking for other maxima. To avoid collisions between the UAVs during the mission, a controller is presented which enables collision avoidance while tracking the particles.

Keywords: Lyapunov stability, autonomous control, nonlinear control systems, obstacle avoidance, gradient methods, potentials.

1. INTRODUCTION

Dynamic tracking of particles is of great importance to Earth Science missions, both as to validate particle transport models and to better understand the interactions in the atmosphere. It is well known that as particle concentrations dissipate, they break down into smaller patches. Using multiple UAVs to perform *in-situ* measurements, it is possible to track these patches as they move with the wind. This will enable real-time information about the exact position of the patches, which can serve as input to update particle transport models with new initial conditions. With a formation of UAVs it is possible to obtain 3D measurements of the particle density, which enables us to find the gradient toward the closest patch with high particle concentration. By following the gradient, the UAVs can locate these patches and enter a circular holding pattern around them. After converging to the holding pattern, one UAV will remain, while the other UAVs continue searching for other patches.

Using the gradient information for guidance and control was first proposed in Khatib (1986), and has since resulted in a large amount of papers (*cf.* Koren and Borenstein (1991), Rimon and Koditschek (1992), Kim and Khosla (1992), Kyriakopoulos et al. (1995), Ge and Cui (2000), Paul et al. (2008), Chunyu et al. (2009), Qu (2009), Siciliano et al. (2010) and references therein). This method is known as the potential field method, and it creates an attractive potential towards the desired position, and can create repulsive potentials around obstacles. By taking the control signal equal to the negative gradient of the resulting field, it enables the UAV to converge to its desired position while avoiding collision with obstacles.

The problem of using UAVs to perform *in-situ* measurements is very interesting and has resulted in many papers on the subject such as Kuroki et al. (2010), Wegener et al. (2004), Šmídl and Hofman (2013), where it is argued that using multiple UAVs as a mobile sensor network will be less expensive and more accurate than what ground-based sensors are able to provide. In Subchan et al. (2008) the problem of tracking a cloud of contaminant was studied, and where they propose an algorithm to track the contaminant cloud based on waypoints to map the entry and exit points of the cloud to track the cloud itself.

In this paper, guidance laws are derived for tracking particle clouds and collision avoidance laws are implemented to avoid collisions between UAVs. It is assumed that the same wind vector affects all particles such that there is zero relative movement of the particles in the wind frame. Using the guidance laws, a virtual leader is designed to represent the desired trajectory, while a group of followers track trajectories relative the virtual leader in a fixed formation. Due to the possibility of a collision when working with multiple UAVs, a reactive controller is presented that makes sure that the UAVs converge to their desired trajectories while avoiding collisions.

2. MODELING

2.1 Notation

In this paper the time derivative of a vector is denoted as $\dot{\mathbf{x}} = d\mathbf{x}/dt$ and the Euclidean length is written as $||\mathbf{x}|| = (\mathbf{x}^\top \mathbf{x})^{\frac{1}{2}}$. Superscript denote the reference frame of the current vector, where n denotes the North East Down (NED) frame, w denotes the wind frame, l denotes the leader frame and v denotes the velocity frame of each follower. The NED frame, assumed to be inertial, has its $\mathbf{x}^n$-axis aligned towards the North, $\mathbf{y}^n$ is pointing East and $\mathbf{z}^n$ is pointing towards the center of the Earth. The wind frame is aligned with the wind vector, the leader frame is defined through the orientation of the virtual leader and the velocity frame is aligned with the velocity vector of each of the followers. The rotation matrix is defined as $\mathbf{R}_a^c \in SO(3)$ which rotates a vector from frame

⋆ This work was supported by the Norwegian Research Council and is part of the Arctic Earth Observation project 195143/I60.

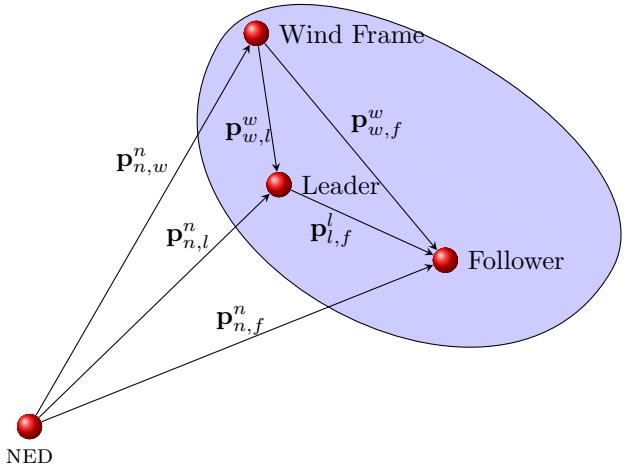

Fig. 1. Reference Frames

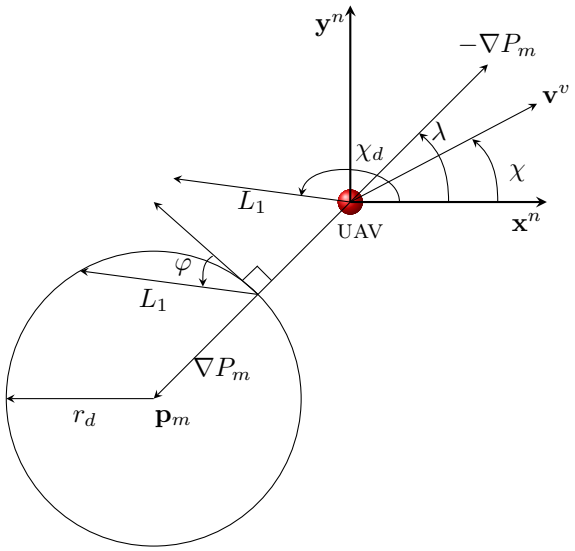

Fig. 2. Guidance Law

a to frame c, where its transpose $(\mathbf{R}^c_a)^\top = \mathbf{R}^a_c$, such that $(\mathbf{R}^a_c)^\top \mathbf{R}^a_c = \mathbf{R}^c_a \mathbf{R}^a_c = \mathbf{I}$, where $\mathbf{I}$ is the identity matrix. The angular velocity vector is denoted $\boldsymbol{\omega}^c_{a,e}$ which represents the angular velocity of frame e relative frame a referenced in frame c, and angular velocities between different frames can be added as $\boldsymbol{\omega}^e_{a,d} = \boldsymbol{\omega}^e_{a,c} + \boldsymbol{\omega}^e_{c,d}$. The time derivative of the rotation matrix is found as $\dot{\mathbf{R}}^c_a = \mathbf{R}^c_a \mathbf{S}(\boldsymbol{\omega}^a_{c,a})$ where the cross-product operator $\mathbf{S}(\cdot)$ is such that for two arbitrary vectors $\mathbf{v}_1, \mathbf{v}_2 \in \mathbb{R}^3$ we have that $\mathbf{S}(\mathbf{v}_1)\mathbf{v}_2 = \mathbf{v}_1 \times \mathbf{v}_2$. The cross-product operator also holds the properties that $\mathbf{S}(\mathbf{v}_1)\mathbf{v}_2 = -\mathbf{S}(\mathbf{v}_2)\mathbf{v}_1$, $\mathbf{S}(\mathbf{v}_1)\mathbf{v}_1 = \mathbf{0}$ and that $\mathbf{v}_1^\top \mathbf{S}(\mathbf{v}_2)\mathbf{v}_1 = 0$. Given $\mathbf{v}_1 = [v_1\ v_2\ v_3]^\top$, the cross-product operator is defined as

$$\mathbf{S}(\mathbf{v}_1) := \begin{bmatrix} 0 & -v_3 & v_2 \\ v_3 & 0 & -v_1 \\ -v_2 & v_1 & 0 \end{bmatrix}. \tag{1}$$

2.2 Formation Flight

The problem of controlling a formation relative a particle cloud that is moving with the wind can be decomposed into two subproblems. The first problem is to design a a virtual leader that tracks the patches in the wind frame, which will be done through the guidance. The resulting trajectory can then be written relative the NED frame which can be used to generate desired trajectories for the followers such that they maintain a rigid formation while tracking the high particle density patches. The wind is assumed to have a constant velocity in a fixed direction, such that $\mathbf{R}^n_w$ and $\mathbf{v}^n_{n,w}$ are known constants. From Fig. 1 we see that

$$\mathbf{p}^n_{n,l} = \mathbf{p}^n_{n,w} + \mathbf{R}^n_w \mathbf{p}^w_{w,l} \tag{2}$$
$$\mathbf{v}^n_{n,l} = \mathbf{v}^n_{n,w} + \mathbf{R}^n_w \mathbf{v}^w_{w,l} \tag{3}$$
$$\mathbf{a}^n_{n,l} = \mathbf{R}^n_w \mathbf{a}^w_{w,l} \tag{4}$$

which produce the trajectory of the virtual leader relative the NED frame. Desiring a rigid formation, meaning that $\mathbf{p}^l_{l,f}$ is a constant displacement away from the virtual leader, the followers trajectories can be found as

$$\mathbf{p}^n_{n,f} = \mathbf{p}^n_{n,l} + \mathbf{R}^n_l \mathbf{p}^l_{l,f} \tag{5}$$
$$\mathbf{v}^n_{n,f} = \mathbf{v}^n_{n,l} + \mathbf{R}^n_l \mathbf{S}(\boldsymbol{\omega}^l_{n,l})\mathbf{p}^l_{l,f} \tag{6}$$
$$\mathbf{a}^n_{n,f} = \mathbf{a}^n_{n,l} + \mathbf{R}^n_l \mathbf{S}^2(\boldsymbol{\omega}^l_{n,l})\mathbf{p}^l_{l,f} + \mathbf{R}^n_l \mathbf{S}(\dot{\boldsymbol{\omega}}^l_{n,l})\mathbf{p}^l_{l,f}, \tag{7}$$

where $\boldsymbol{\omega}^l_{n,l}$ and $\dot{\boldsymbol{\omega}}^l_{n,l}$ are the angular velocity and acceleration of the virtual leader relative the NED frame. Since the wind is moving in a constant direction, $\boldsymbol{\omega}^l_{n,w} = \mathbf{0}$ and it follows that $\boldsymbol{\omega}^l_{n,l} = \boldsymbol{\omega}^l_{n,w} + \boldsymbol{\omega}^l_{w,l} = \boldsymbol{\omega}^l_{w,l}$. Inserting (2)-(4) into (5)-(7), and defining $\mathbf{p}^n_{d,i} := \mathbf{p}^n_{w,f}$, $\mathbf{v}^n_{d,i} := \mathbf{v}^n_{w,f}$, and $\mathbf{a}^n_{d,i} := \mathbf{a}^n_{w,f}$, the desired trajectory of the i'th follower becomes

$$\mathbf{p}^n_{d,i} = \mathbf{p}^n_{n,w} + \mathbf{R}^n_w \mathbf{p}^w_{w,l} + \mathbf{R}^n_l \mathbf{p}^l_{l,f} \tag{8}$$
$$\mathbf{v}^n_{d,i} = \mathbf{v}^n_{n,w} + \mathbf{R}^n_w \mathbf{v}^w_{w,l} + \mathbf{R}^n_l \mathbf{S}(\boldsymbol{\omega}^l_{n,l})\mathbf{p}^l_{l,f} \tag{9}$$
$$\mathbf{a}^n_{d,i} = \mathbf{R}^n_w \mathbf{a}^w_{w,l} + \mathbf{R}^n_l \mathbf{S}^2(\boldsymbol{\omega}^l_{n,l})\mathbf{p}^l_{l,f} + \mathbf{R}^n_l \mathbf{S}(\dot{\boldsymbol{\omega}}^l_{n,l})\mathbf{p}^l_{l,f}. \tag{10}$$

3. GUIDANCE

Using sensor measurements of the particle density it is possible to find the gradient ∇P_m towards the closest patch of particles as shown in Fig. 2. We wish the UAVs to enter a circular holding pattern around the point with the highest density, $\mathbf{p}_m$ at a fixed radius, r_d. The heading of the UAV is denoted χ, χ_d is the desired heading, λ is the line of sight angle, ϕ is the angle between the tangent of the circle and the look-ahead-distance L_1, which is used to smoothen the convergence to the circle. Proportional Navigation (PN) is a very popular guidance law used for tactical missile guidance systems. The PN guidance law for intercepting a stationary target in the xy-plane is given by Guelman (1971) as

$$a_\chi = NV\dot{\lambda} = -\frac{NV^2 \sin(\chi - \chi_d)}{r} \tag{11}$$

where N is the navigation constant, V is the total velocity, r is the distance between the missile/UAV and the target, and $\dot{\lambda}$ is the line of sight rate. This guidance law can be modified to make the UAV converge to a circle around a given point as discussed in the work by Narayanachar and Kristiansen (2012). Selecting $N = 2$, and using a constant

look-ahead-distance, L_1 instead of r, the acceleration command becomes

$$a_\chi = -\frac{2V^2 \sin(\chi - \chi_d)}{L_1}. \tag{12}$$

By studying Fig. 2 we see that $\chi_d = \lambda + \frac{\pi}{2} + \phi$ where $\phi = \sin^{-1}(L_1/2r_d)$. After inserting this, the acceleration command which will make the UAV enter a circular trajectory around a maximum is given as

$$a_\chi = -\frac{2V^2 \cos(\chi - \lambda - \phi)}{L_1}. \tag{13}$$

Similarly as in the xy plane, a guidance law for the altitude can be chosen as

$$a_\gamma = -\frac{2V^2 \sin(\gamma - \gamma_d)}{L_2} \tag{14}$$

where L_2 is another look-ahead constant, γ is the flight path angle while γ_d is the desired flight path angle. Let the reference heading rate and flight path rate be defined as

$$\dot{\chi}_r = \frac{a_\chi}{V} \qquad \dot{\gamma}_r = \frac{a_\gamma}{V} \tag{15}$$

which can be used as input to the first order filters

$$\ddot{\chi} = -\frac{1}{T_\chi}(\dot{\chi} - \dot{\chi}_r) \tag{16}$$

$$\ddot{\gamma} = -\frac{1}{T_\gamma}(\dot{\gamma} - \dot{\gamma}_r) \tag{17}$$

to produce the second derivative of the heading and flight path angle where $T_\chi, T_\gamma > 0$. The angular velocity in wind frame can be found as

$$\boldsymbol{\omega}^l_{w,l} = \begin{bmatrix}0\\ \dot{\gamma}\\ 0\end{bmatrix} + \begin{bmatrix}\cos(\gamma) & 0 & -\sin(\gamma)\\ 0 & 1 & 0\\ \sin(\gamma) & 0 & \cos(\gamma)\end{bmatrix}\begin{bmatrix}0\\ 0\\ \dot{\chi}\end{bmatrix} = \begin{bmatrix}-\dot{\chi}\sin(\gamma)\\ \dot{\gamma}\\ \dot{\chi}\cos(\gamma)\end{bmatrix} \tag{18}$$

where the angular acceleration is found through differentiation as

$$\dot{\boldsymbol{\omega}}^l_{w,l} = \begin{bmatrix}-\ddot{\chi}\sin(\gamma) - \dot{\chi}\dot{\gamma}\cos(\gamma)\\ \ddot{\gamma}\\ \ddot{\chi}\cos(\gamma) - \dot{\chi}\dot{\gamma}\sin(\gamma)\end{bmatrix}. \tag{19}$$

A kinematic model of the virtual leader can now be defined relative the wind frame as

$$\mathbf{v}^w_{w,l} = \begin{bmatrix}V\cos(\chi)\cos(\gamma)\\ V\sin(\chi)\cos(\gamma)\\ -V\sin(\gamma)\end{bmatrix} \tag{20}$$

which can be differentiated assuming that the total velocity is constant resulting in the acceleration as

$$\mathbf{a}^w_{w,l} = \begin{bmatrix}-V\sin(\chi)\cos(\gamma)\dot{\chi} - V\cos(\chi)\sin(\gamma)\dot{\gamma}\\ V\cos(\chi)\cos(\gamma)\dot{\chi} - V\sin(\chi)\sin(\gamma)\dot{\gamma}\\ -V\cos(\gamma)\dot{\gamma}\end{bmatrix}, \tag{21}$$

and the rotation matrix from the leader frame to the wind frame can be defined as

$$\mathbf{R}^w_l = \begin{bmatrix}\cos\chi & -\sin(\chi) & 0\\ \sin(\chi) & \cos(\chi) & 0\\ 0 & 0 & 1\end{bmatrix}\begin{bmatrix}\cos(\gamma) & 0 & \sin(\gamma)\\ 0 & 1 & 0\\ -\sin(\gamma) & 0 & \cos(\gamma)\end{bmatrix}, \tag{22}$$

enabling the rotation from the leader frame to NED frame to be found as $\mathbf{R}^n_l = \mathbf{R}^n_w \mathbf{R}^w_l$.

3.1 Modeling the Particle Cloud

The guidance require the line of sight angle λ, and the desired flight path angle γ_d which can be found by studying the gradient of the particle cloud. A particle cloud contains multiple patches with high density relative the surrounding air. To model the particle distribution a Gaussian function is applied from each of the maximum points as

$$P_{m,i} = \frac{1}{2} A \exp\left(-\frac{1}{\sigma^2}||\mathbf{p}^w_{w,l} - \mathbf{p}^w_{m,i}||^2\right) \tag{23}$$

where A is the amplitude, $\mathbf{p}^w_{w,l}$ is the position of the virtual leader, $\mathbf{p}^w_{m,i}$ is the i'th maximum point, σ^2 is the variance, and the gradient of the Gaussian function is found as

$$\nabla P_{m,i} = -\frac{A}{\sigma^2}(\mathbf{p}^w_{w,l} - \mathbf{p}^w_{m,i}) \exp\left(-\frac{1}{\sigma^2}||\mathbf{p}^w_{w,l} - \mathbf{p}^w_{m,i}||^2\right). \tag{24}$$

Since there are multiple patches containing high density, the gradient of the total attractive field is found as $\nabla P_m = \sum_{i=1}^{N} \nabla P_{m,i}$, which can be used to find the line-of-sight vector towards the closest maximum. Defining $\begin{bmatrix}\frac{\partial P_m}{\partial x} & \frac{\partial P_m}{\partial y} & \frac{\partial P_m}{\partial z}\end{bmatrix}^\top = \frac{\nabla P_m}{||\nabla P_m||}$ the line of sight angle and the desired flight path angle are found as

$$\lambda = \tan^{-1}\left(\frac{\frac{\partial P_m}{\partial y}}{\frac{\partial P_m}{\partial x}}\right) - \pi \tag{25}$$

$$\gamma_d = -\sin^{-1}\left(\frac{\partial P_m}{\partial z}\right). \tag{26}$$

These angles can then be inserted into the guidance laws (13) and (14) providing the acceleration commands which will make the virtual leader converge to a circular trajectory around the maximum at a given altitude. After converging to the circular holding pattern, one of the UAVs shall remain, while the other UAVs go searching for other maxima. This can be done by placing a repulsive field, $\nabla P_{r,i} = -\nabla P_{m,i}$ at the maximum to cancel out the attractive potential. By letting this repulsive field affect all but the UAV which remain, it will make the other UAVs go looking for other maxima. The exact position of the maximum point can be found by using $\mathbf{p}^w_{m,i} = \mathbf{p}^w_{w,l} + r_d \frac{\nabla P_m}{||\nabla P_m||}$.

4. MODEL OF THE THE FOLLOWERS

Let the model of the follower UAVs be given by the double integrator

$$\dot{\mathbf{p}}^n_{n,f} = \mathbf{v}^n_{n,f} \tag{27}$$

$$\dot{\mathbf{v}}^n_{n,f} = \mathbf{a}^n_{n,f} \tag{28}$$

with attitude kinematics as

$$\dot{\mathbf{R}}^n_v = \mathbf{R}^n_v \mathbf{S}(\boldsymbol{\omega}^v_{n,v}) \tag{29}$$

where $\boldsymbol{\omega}^v_{n,v} := [p\ q\ r]^\top$ and $||\boldsymbol{\omega}^v_{n,v}|| \leq \omega_{max}$ where ω_{max} is a bound on the angular rates. , and noting that the total velocity in the velocity frame is aligned with the $\mathbf{x}^v$ axis, enables the model to be written as

$$\dot{\mathbf{p}}^n_{n,f} = \mathbf{R}^n_v \mathbf{v}^v = \mathbf{R}^n_v \begin{bmatrix}V\\ 0\\ 0\end{bmatrix} \tag{30}$$

$$\dot{\mathbf{v}}^n_{n,f} = \mathbf{R}^n_v \mathbf{S}(\boldsymbol{\omega}^v_{n,v}) \begin{bmatrix}V\\ 0\\ 0\end{bmatrix} + \mathbf{R}^n_v \begin{bmatrix}\dot{V}\\ 0\\ 0\end{bmatrix}. \tag{31}$$

Let the control variables of the UAV be defined as $\mathbf{u}^v = \begin{bmatrix}\dot{V} & q & r\end{bmatrix}^\top$, then the acceleration can be rewritten as

$$\dot{\mathbf{v}}^n_{n,f} = \mathbf{R}^n_v \mathbf{B} \mathbf{u}^v \tag{32}$$

where

$$\mathbf{B} = \begin{bmatrix} 1 & 0 & 0 \\ 0 & 0 & V \\ 0 & -V & 0 \end{bmatrix} \tag{33}$$

which has full rank as long as the total velocity is larger than zero.

Remark 1. In order to make the system controllable without angular singularities, we have exploited the properties of the rotation matrix producing the angular velocities. If we had used a similar model as for the virtual leader (21), it would have been singular if the flight path angle had been equal to $\pm\pi/2$.

5. COLLISION AVOIDANCE

During the mission it is vital that no collisions occur and a controller that ensures this will be derived based on the artificial potential field method. This section is based on the work by Oland and Kristiansen (2013) where the resulting controller was applied to collision and terrain avoidance for a formation of fixed-wing UAVs. The position of the i'th UAV can be defined as $\mathbf{p}_i := \mathbf{p}^n_{n,f}$, and the position of a j'th UAV can be treated as an obstacle, denoted $\mathbf{p}_{o,j}$. The objective is to design a controller for each of the followers, where we define $\mathbf{a}_i := \dot{\mathbf{v}}^n_{n,f} := \mathbf{u}_i$ as the control signal in the NED frame, which then can be transformed to the velocity frame for the individual follower by inverting (32), giving

$$\mathbf{u}^v_i = \mathbf{B}^{-1} \mathbf{R}^v_n \mathbf{u}_i \tag{34}$$

where $\mathbf{u}_i$ is to be designed.

The controller which is derived in this section is based on the artificial potential field method. The total potential field consists of two types of potentials, an attractive potential which will force the UAVs to their desired trajectories, and a set of repulsive potentials which will force the UAVs away from the other UAVs. The combined potential will make the UAVs converge to their trajectories while avoiding collisions.

Remark 2. The artificial potential field method has several inherent limitations as discussed in Koren and Borenstein (1991). When an obstacle is directly between a mobile robot and its desired position, a local minimum will be created. The mobile robot will then converge to a position which is not its desired position, but will become stuck at the local minimum. In the case of UAVs where they are treated as obstacles for each other, local saddle points will arise, which may result in undesirable motion, but since the UAVs and the desired trajectories are nonstationary, they will never become stuck at a saddle point.

5.1 Attractive Potential

The attractive potential for the i'th UAV can be defined using a paraboloidal and a conical potential as shown in Siciliano et al. (2010) where

$$P_a = \begin{cases} \frac{1}{2} k_a ||\mathbf{p}_i - \mathbf{p}_{d,i}||^2 & \text{if } ||\mathbf{p}_i - \mathbf{p}_{d,i}|| \leq r_a \\ k_a ||\mathbf{p}_i - \mathbf{p}_{d,i}|| & \text{otherwise} \end{cases} \tag{35}$$

with the gradient of the attractive potential as

$$\nabla P_a = \begin{cases} k_a (\mathbf{p}_i - \mathbf{p}_{d,i}) & \text{if } ||\mathbf{p}_i - \mathbf{p}_{d,i}|| \leq r_a \\ k_a \dfrac{(\mathbf{p}_i - \mathbf{p}_{d,i})}{||\mathbf{p}_i - \mathbf{p}_{d,i}||} & \text{otherwise.} \end{cases} \tag{36}$$

Here k_a denotes the attractive gain while $\mathbf{p}_i$ and $\mathbf{p}_{d,i}$ denote the current position and desired position of the i'th UAV. The radius r_a denotes the boundary where we switch between the paraboloidal attractive potential (first) and the conical attractive potential (second). The reason for this switching is to obtain a bounded attractive force as well as to avoid the singularity of the conical attractive potential when the UAV is in its desired position. By defining the radius $r_a = 1$, the intersection between the paraboloidal and the conical potentials is at the unit sphere, and thus we obtain a continuous attractive potential function for all $\mathbf{p}_i \in \mathbb{R}^3$.

5.2 Repulsive Potential

The repulsive field for the j'th obstacle can be defined as

$$P_{r,j} = \begin{cases} \frac{1}{2} k_r \left(\dfrac{1}{||\mathbf{p}_i - \mathbf{p}_{o,j}||} - \dfrac{1}{r_o} \right)^2 & \text{if } ||\mathbf{p}_i - \mathbf{p}_{o,j}|| < r_o \\ 0 & \text{otherwise} \end{cases} \tag{37}$$

with its gradient as

$$\nabla P_{r,j} = \begin{cases} \dfrac{-k_r (\mathbf{p}_i - \mathbf{p}_{o,j})}{||\mathbf{p}_i - \mathbf{p}_{o,j}||^3} \left(\dfrac{1}{||\mathbf{p}_i - \mathbf{p}_{o,j}||} - \dfrac{1}{r_o} \right) & \text{if } ||\mathbf{p}_i - \mathbf{p}_{o,j}|| < r_o \\ 0 & \text{otherwise.} \end{cases}$$

Here the repulsive gain is denoted k_r, the position of the j'th obstacle is denoted $\mathbf{p}_{o,j}$ and the radius r_o denotes the sphere of influence where the repulsive potential becomes active.

5.3 Total Field

The total potential field is found as the sum of the attractive field and repulsive fields

$$P = P_a + \sum_{j=1}^{M} P_{r,j} \tag{38}$$

which can be used to define a controller equal to the negative gradient of the total field where the gradient is defined as

$$\nabla P = \begin{bmatrix} \dfrac{\partial P}{\partial x_i} & \dfrac{\partial P}{\partial y_i} & \dfrac{\partial P}{\partial z_i} \end{bmatrix}^\top \tag{39}$$

which will enable a UAV to avoid obstacles and converge to a desired position.

Remark 3. The attractive potential does not take velocity into account, and thus it is similar to a simple P-controller which will result in oscillations around its desired trajectory. We have chosen to add the velocity feedback in the reactive controller, but it is worth to mention that it can be included directly in the attractive potential.

Remark 4. This controller does not take into account the velocity and acceleration of other UAVs, which must be done in order to avoid collisions in a dynamic environment.

5.4 Controller

The controller is based on the work by Qu (2009) and takes the velocity and acceleration of other UAVs into

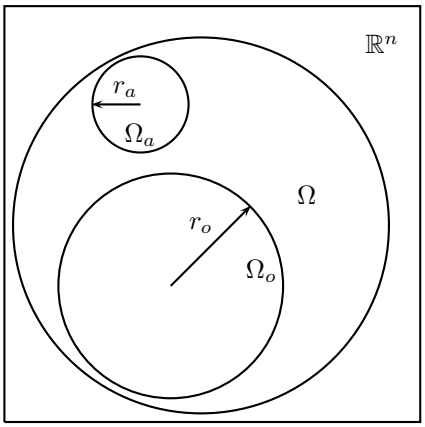

Fig. 3. Sets used for stability analysis

account when calculating the control signal required to avoid collisions and converge to its desired trajectory.

The controller is defined as

$$\begin{aligned}\mathbf{u}_i :=& \mathbf{a}_i = \mathbf{a}_{d,i} - k\sum_{j=1}^{M} \nabla^2 P_{r,j}(\mathbf{v}_i - \mathbf{v}_{o,j})||\mathbf{v}_{d,i} - \mathbf{v}_{o,j}||^2 \\ &- 2k\sum_{j=1}^{M} \nabla P_{r,j}(\mathbf{v}_{d,i} - \mathbf{v}_{o,j})^\top(\mathbf{a}_{d,i} - \mathbf{a}_{o,j}) \\ &- \xi_i(\mathbf{v}_i - \mathbf{v}_{d,i}) - \nabla P_a - \sum_{j=1}^{M} \nabla P_{r,j} \end{aligned} \tag{40}$$

where ξ_i is a positive function that becomes zero in the set Ω_o and $k > 0$ is a constant and $\nabla^2 P_{r,j}$ is the Hessian matrix and is given in Appendix A. Let the operational set be defined as $\Omega \subset \mathbb{R}^3$, and two subsets as

$$\Omega_a = \{\mathbf{p}_i \in \Omega \mid ||\mathbf{p}_i - \mathbf{p}_{d,i}|| \leq r_a\} \tag{41}$$

$$\Omega_o = \{\mathbf{p}_i \in \Omega \mid ||\mathbf{p}_i - \mathbf{p}_{o,j}|| \leq r_o\} \tag{42}$$

where r_a is the radius of the attractive set, r_o the radius of the obstacle set and the sets are illustrated in Fig. 3. In the set $\Omega \setminus (\Omega_a \cup \Omega_o)$ the conic potential is active, producing a bounded attractive force moving the UAV towards the attractive set Ω_a. Once inside Ω_a the paraboloidal potential becomes active and forces the UAV into its desired position. If the UAV enters the obstacle set, Ω_o during its maneuver, the repulsive potential will push the UAV back to the set $\Omega \setminus (\Omega_a \cup \Omega_o)$ from where it will continue towards Ω_a. The stability of the closed loop system is shown in Oland and Kristiansen (2013) to be uniformly asymptotically stable in the sets Ω_a and $\Omega \setminus (\Omega_a \cup \Omega_o)$; and uniformly stable in Ω_o meaning that no collisions will occur.

6. SIMULATION

Three UAVs start with three arbitrary positions, marked with square boxes as shown in Fig. 4. The followers have the following positions relative the virtual leader: $\mathbf{p}^l_{l,f1} = [0\ 0\ 0]^\top$, $\mathbf{p}^l_{l,f2} = [-20\ -20\ 0]^\top$ and $\mathbf{p}^l_{l,f3} = [-20\ 20\ 0]^\top$ which results in a triangular formation. Initially they do not know where they are going, but by performing measurements, they converge to their formation and follow the gradient to the closest maximum which is located at

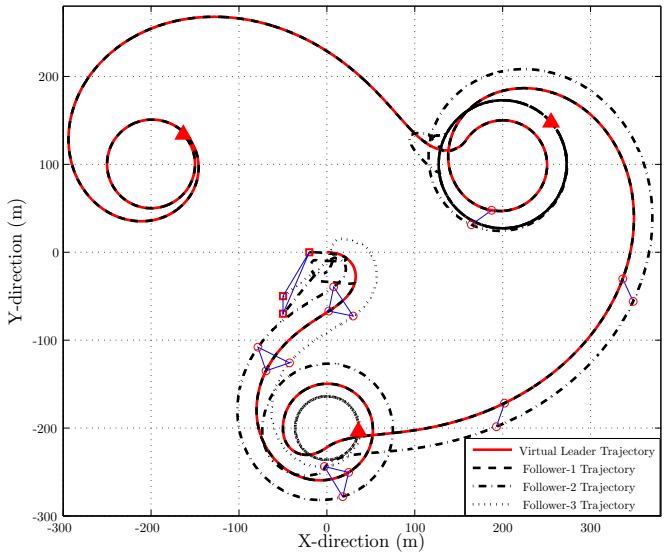

Fig. 4. Flight path of the UAVs in the xy-plane of the wind frame.

$(0, -200)$. After converging towards the first maximum, Follower-1 and the Follower-2 continue searching for other maxima, while Follower-3 remains in a holding pattern around the first maximum point. The two UAVs continue with a reduced formation before they find the second maximum at $(200, 100)$, where Follower-2 remains while Follower-1 continue to find the last maximum point at $(-200, 100)$. The final positions of the UAVs at the end of the simulation are shown with triangles.

By looking closely at Fig. 4 it can be seen that there is chaotic movement before the UAVs converge to their trajectories, as well as when Follower-1 is moving away from the second maximum. This is a result of the collision avoidance method where the UAVs avoid collision with each other. The radius of the repulsive field has been defined to be $r_o = 20m$, which can be seen in Fig. 5, where no UAVs come closer than $20m$.

Remark 5. Using a formation of UAVs, 3D measurements can be used to find the gradient toward the closest maximum. When Follower-1 is flying alone, it is assumed that it has an observer which provides an estimate of the gradient.

7. CONCLUSION

In this paper a solution to the problem of real time particle tracking has been presented. The result shows that even though the UAVs do not know where they are going, they are able to find the patches with highest particle density based on sensor measurements providing the gradient of the resulting field. From the simulation it is shown that the followers are able to track the virtual leader without colliding with each other and converge to circular holding patterns around the three high density particle patches. The basic idea of using potential field to guide an unmanned aerial vehicle to track particles, can easily be extended to autonomous mapping of an area by defining multiple points of interest. As the UAVs pass close to a given point, a repulsive field can be erected, forcing the UAVs to continue its mapping operation.

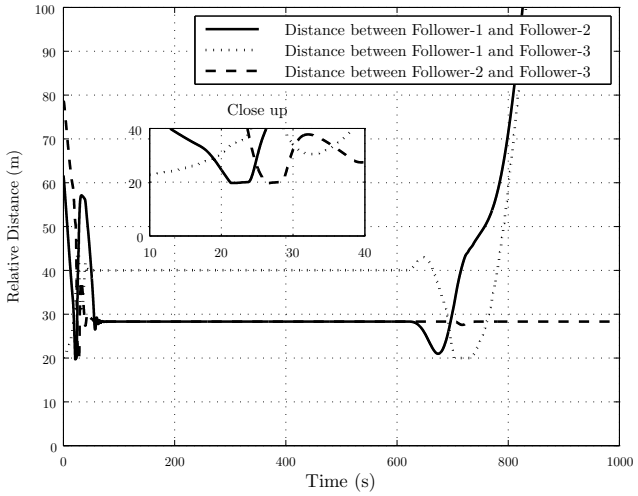

Fig. 5. Relative distance between the UAVs

Appendix A. HESSIAN MATRIX

With $\tilde{\mathbf{p}} := \mathbf{p}_i - \mathbf{p}_{o,j} = [\tilde{x}\ \tilde{y}\ \tilde{z}]^\top$ the Hessian matrix for the repulsive field is found as

$$\nabla^2 P_r = k_r \begin{bmatrix} a_{11} & a_{12} & a_{13} \\ a_{21} & a_{22} & a_{23} \\ a_{31} & a_{32} & a_{33} \end{bmatrix} \tag{A.1}$$

$$a_{11} = \frac{\tilde{x}^2}{||\tilde{\mathbf{p}}||^6} + \frac{3\tilde{x}^2}{||\tilde{\mathbf{p}}||^5}\left(\frac{1}{||\tilde{\mathbf{p}}||} - \frac{1}{r_o}\right) - \frac{1}{||\tilde{\mathbf{p}}||^3}\left(\frac{1}{||\tilde{\mathbf{p}}||} - \frac{1}{r_o}\right)$$
$$a_{12} = \frac{\tilde{x}\tilde{y}}{||\tilde{\mathbf{p}}||^6} + \frac{3\tilde{x}\tilde{y}}{||\tilde{\mathbf{p}}||^5}\left(\frac{1}{||\tilde{\mathbf{p}}||} - \frac{1}{r_o}\right)$$
$$a_{13} = \frac{\tilde{x}\tilde{z}}{||\tilde{\mathbf{p}}||^6} + \frac{3\tilde{x}\tilde{z}}{||\tilde{\mathbf{p}}||^5}\left(\frac{1}{||\tilde{\mathbf{p}}||} - \frac{1}{r_o}\right)$$
$$a_{21} = \frac{\tilde{x}\tilde{y}}{||\tilde{\mathbf{p}}||^6} + \frac{3\tilde{x}\tilde{y}}{||\tilde{\mathbf{p}}||^5}\left(\frac{1}{||\tilde{\mathbf{p}}||} - \frac{1}{r_o}\right)$$
$$a_{22} = \frac{\tilde{y}^2}{||\tilde{\mathbf{p}}||^6} + \frac{3\tilde{y}^2}{||\tilde{\mathbf{p}}||^5}\left(\frac{1}{||\tilde{\mathbf{p}}||} - \frac{1}{r_o}\right) - \frac{1}{||\tilde{\mathbf{p}}||^3}\left(\frac{1}{||\tilde{\mathbf{p}}||} - \frac{1}{r_o}\right)$$
$$a_{23} = \frac{\tilde{y}\tilde{z}}{||\tilde{\mathbf{p}}||^6} + \frac{3\tilde{y}\tilde{z}}{||\tilde{\mathbf{p}}||^5}\left(\frac{1}{||\tilde{\mathbf{p}}||} - \frac{1}{r_o}\right)$$
$$a_{31} = \frac{\tilde{x}\tilde{z}}{||\tilde{\mathbf{p}}||^6} + \frac{3\tilde{x}\tilde{z}}{||\tilde{\mathbf{p}}||^5}\left(\frac{1}{||\tilde{\mathbf{p}}||} - \frac{1}{r_o}\right)$$
$$a_{32} = \frac{\tilde{y}\tilde{z}}{||\tilde{\mathbf{p}}||^6} + \frac{3\tilde{y}\tilde{z}}{||\tilde{\mathbf{p}}||^5}\left(\frac{1}{||\tilde{\mathbf{p}}||} - \frac{1}{r_o}\right)$$
$$a_{33} = \frac{\tilde{z}^2}{||\tilde{\mathbf{p}}||^6} + \frac{3\tilde{z}^2}{||\tilde{\mathbf{p}}||^5}\left(\frac{1}{||\tilde{\mathbf{p}}||} - \frac{1}{r_o}\right) - \frac{1}{||\tilde{\mathbf{p}}||^3}\left(\frac{1}{||\tilde{\mathbf{p}}||} - \frac{1}{r_o}\right).$$

REFERENCES

Chunyu, J., Qu, Z., P., E., and Falash, M. (2009). A New Reactive Target-Tracking Control with Obstacle Avoidance in a Dynamic Environment. In *Proceedings of the American Control Conference*.

Ge, S.S. and Cui, Y.J. (2000). New Potential Functions for Mobile Robot Path Planning. *IEEE Transactions on Robotics and Automation*, Vol. 16, No. 5, 615–620.

Guelman, M. (1971). A qualitative study of proportional navigation. *IEEE Transaction on Aerospace and Electronic Systems*, Vol. 7, No. 4, 637–643.

Khatib, O. (1986). Real-Time Obstacle Avoidance for Manipulators and Mobile Robots. *The International Journal of Robotics Research*, Vol 5. No. 1, 90–98.

Kim, J. and Khosla, P.K. (1992). Real-Time Obstacle Avoidance Using Harmonic Potential Functions. *IEEE Transactions on Robotics and Automation*, Vol. 8, No. 3, 338–349.

Koren, Y. and Borenstein, J. (1991). Potential Field Methods and Their Inherent Limitations for Mobile Robot Navigation. In *Proceedings of the IEEE Conference on Robotics and Automation*.

Kuroki, Y., Young, G.S., and Haupt, S.E. (2010). UAV navigation by an expert system for contaminant mapping with a genetic algorithm. *Exptert Systems with Applications*, Vol. 37, No. 6, 4687–4697.

Kyriakopoulos, K.J., Kakambouras, P., and Krikelis, N.J. (1995). Potential Fields for Nonholonomic Vehicles. In *Proceedings of the 1995 IEEE Symposium on Intelligent Control*.

Narayanachar, D. and Kristiansen, R. (2012). Guidance Strategy for Gradient Search by Multiple UAVs. In *Proceedings of the AIAA Guidance, Navigation and Control Conference (GNC), Minneapolis, MN.*

Oland, E. and Kristiansen, R. (2013). Collision and Terrain Avoidance for UAVs using the Potential Field Method. In *Proceedings of the IEEE Aerospace Conference, Big Sky, Montana*.

Paul, T., Krogstad, T.R., and Gravdahl, J.T. (2008). Modelling of UAV formation flight using 3D potential field. *Simulation Modelling Practice and Theory*, Vol. 16, No. 9, 1453–1462.

Qu, Z. (2009). *Cooperative Control of Dynamical Systems*. Springer-Verlag London Limited.

Rimon, E. and Koditschek, D.E. (1992). Exact Robot Navigation Using Artificial Potential Functions. *Transactions on Robotics and Automation*, Vol. 8, No. 5, 501 – 518.

Siciliano, B., Sciavicci, L., Villani, L., and Oriolo, G. (2010). *Robotics Modelling, Planning and Control*. Springer.

Šmídl, V. and Hofman, R. (2013). Tracking of atmospheric release of pollution using unmanned aerial vehicles. *Atmospheric Environment*, Vol. 67, 1–12.

Subchan, S., White, B., Tsourdos, A., Shanmugavel, M., and Zbikowski, R. (2008). Dubins Path Planning of Multiple UAVs for Tracking Contaminant Cloud. In *Proceedings of the 17th IFAC World Congress*.

Wegener, S.S., Schoenung, S.M., Totah, J., Sullivan, D., Frank, J., Enomoto, F., Frost, C., and Theodore, C. (2004). UAV Autonomous Operations for Airborne Science Missions. In *AIAA 3rd Unmanned Unlimited Technical Conference, Workshop and Exhibit, 110.*